Isothermal annealing of a cold-rolled Al-Mn-Fe-Si alloy with different microchemistry states

HUANG Ke (黄科)[1]*, LI Yan-jun (李彦军)[1,2], Knut MARTHINSEN[1],

1. Department of Materials Science and Engineering,
Norwegian University of Science and Technology (NTNU), Trondheim 7491, Norway
2. SINTEF Materials and Chemistry, N-7465, Norway

Abstract: Microstructural evolution of a cold-rolled Al-Mn-Fe-Si alloy during annealing has been studied. Except the as cast variant, two other different homogenizations have been considered, one giving a high density of fine dispersiods providing a considerable Zener drag influencing the softening behavior while the other gives a lower density of coarser dispersoid structure providing a much smaller drag effect. The gradual microstructural evolutions during annealing for the three variants are captured by interrupting annealing at different times. Effects of microchemistry state on recrystallization kinetics, recrystallized grain structure and texture have been characterized in detail by EBSD. It is demonstrated that the actual softening kinetics, final microstructure and texture are a result of delicate balance between processing conditions and microchemistry state. Strong concurrent precipitation takes place for the case with high concentration of Mn in solid solution, which suppresses nucleation and retards recrystallization and finally leads to grain structure of coarse elongated grains dominated by a P texture component together with a ND-rotated cube component. On the contrary, when solute content of Mn is low and pre-existing dispersoids are relatively coarser, faster recrystallization kinetics is exhibited together with an equiaxed grain structure with mainly cube texture.

Key words: Aluminum alloy; recrystallization kinetics; microchemistry; particles; precipitation; texture

1 Introduction

It is well established that particles are of the outmost importance in recrystallization of alloys containing second-phase particles [1-6]. Small and numerous dispersoids (typically formed during homogenization and/or subsequent heat treatments) tend to hinder boundary motion and slow down recrystallization and grain growth through a Zener drag effect [7]. With a sufficiently small spacing of thermally stable particles, it is even possible to preserve the deformed/recovered microstructure up to the melting temperature of the matrix [8]. By contrast, widely spaced coarse constituent particles larger than ~1μm, formed during casting, can accelerate recrystallization by particle stimulated nucleation (PSN) due to the large amount of stored energy that concentrate next to them during cold rolling [9]. It is well documented that a suitable homogenization cycle may strongly facilitate the down-stream recrystallization of Al sheet by providing different microchemistry states (solid solution levels, constituent particles and dispersoids) [10-18]. However, the effects and mechanisms behind are neither well understood nor quantitatively described. The objective of the present work was to

Foundation item: Project (193179/I40) supported by the Research Council of Norway and the industrial partners, Hydro Aluminium and Sapa Technology. NTNU, through the "Strategic Area Materials" is also gratefully acknowledged for financial support to HUANG Ke.
Corresponding author: HUANG Ke; Tel: +47-73594004; E-mail: ke.huang@ntnu.no

investigate the effect of different microchemistry introduced by homogenization on the softening behavior of a cold rolled Al-Mn-Fe-Si alloy. The effect of microchemistry state on the fully recrystallized grain structure and texture has been investigated and presented elsewhere [19]. The focus of the present paper is on identifying the effect of pre-existing dispersoids and concurrent precipitation on the nucleation and subsequent microstructural evolution during isothermal annealing. It is part of a comprehensive investigation on particle-annealing interactions in AA3xxx alloys involving both industrial and academic partners, the objective being to obtain a better understanding of the evolution of microstructure and texture and their interactions with second-phase particles during cold rolling and subsequent annealing of AA 3xxx type alloys [19-27], as basis for validation and further development of relevant microstructure models accounting for these aspects.

2 Experimental

2.1 Alloy conditions and annealing treatment

The investigated alloy was received from Hydro Aluminium as a DC-cast AA3xxx extrusion billet. The as-received material, denoted as C1, were in the as-cast state, with the chemical composition: Mn 0.4 wt %, Fe 0.5 wt%, Si 0.15 wt%. The material possessed grains of equiaxed shape with an average size of ~140μm, more details can be found elsewhere [19-22].

The received C1 material was subsequently homogenized at two different conditions to get different microchemistry, i.e. amount of solute (mainly Mn) and second-phase particle. The homogenization treatments were performed in an air circulation furnace with a temperature accuracy of ±2 K, starting from room temperature (about 20 °C). One set of the samples for C1 were heated at 50^{o}C/h to 450 ^{o}C and kept for 4 hours, referred to as C1-2. Another set of the samples were subjected to a two-stage homogenization treatment. First, the samples were heated at 50^{o}C/h to 600 ^{o}C and held at this temperature for 4 hours, then the samples were cooled at 25 ^{o}C/h to 500^{o}C where they were kept for another 4 hours, which gives the C1-3 condition. The as-cast material is designated as C1-0. Materials were water quenched to room temperature at the end of the homogenization procedure to freeze the state of supersaturation/precipitation potential.

The homogenized materials together with the materials of the as-cast condition, were cold rolled to deformation strain of $\varepsilon = 1.6$. The rolled sheets were subsequently isothermally back-annealed in a pre-heated salt bath at prescribed temperatures and with different holding time in the range of 5-10^{5}s, followed by quick water quenching.

2.2 Microstructure characterization

The softening and precipitation behavior during annealing were followed by Vickers hardness (VHN) and electrical conductivity (EC) measurements performed on the RD-TD plane of sheets. Each reported value was obtained by averaging eight measurements. Electrical conductivity was measured by a Sigmascope EX 8 instrument at room temperature of about 293 K (20°C). It has been observed elsewhere that the concentration of Fe and Si in solid solution of similar alloy are very small and varies little during heat treatment, so it is reasonable to assume the evolution of EC is mainly due to the variation of Mn in solid solution [28]. Thus it can be used as a semi-quantitative measure of the concurrent precipitation of Mn containing particles. Metallographic examinations of constituent particles and dispersoids were carried out by backscattered electron channeling contrast imaging in a Zeiss Ultra 55 field emission gun scanning electron microscope (FEG-SEM). Images were captured electronically and analyzed using standard image analysis software. Characteristic size parameters of constituent particles, equivalent diameter d and number density were measured by the image analysis software Image-J. For the hardness measurements, a load of 1 Kg, a loading time of 15 s and a loading

speed of 100μms^{-1} were used.

The crystallographic textures of the sheets were measured by means of EBSD (Electron backscattered diffraction), by the same Zeiss Supra/Ultra 55 scanning electron microscope (SEM) as mentioned above, and by means of TSL software. Orientation maps of both deformed and annealed samples, covering typically more than one thousand grains (except the cases with extremely large grains), with time step 1-2 μm, were used to study the orientation of the recrystallized grains and thus the texture evolution during recrystallization.

Selected conditions were characterized by SEM/EBSD so that the effect of homogenization and level of Mn in solid solution on the softening behavior in terms of microstructure and texture evolution of the different homogenized conditions could be studied. For all of the micrographs presented in this paper, the horizontal direction corresponds to rolling direction (RD) while the vertical direction is the normal direction (ND). The grain size was measured as the equivalent diameter in the RD-ND cross section. The texture was determined by single grain orientation measurements by EBSD. From the single grain orientation measurements the ODF was calculated by assigning a 15° deviation from the ideal rolling/recrystallization components.

3 Results and discussion

3.1 The microchemistry state before annealing

The micrographs of the particle distribution for the three variants (before deformation) are presented elsewhere [19]. From this work it is clear that the variant homogenized at the lower temperature, i.e. C1-2, obviously has more but finer dispersoids than its counterpart C1-3, as illustrated in Table 1. It is important to note that the dispersoids were shown to have a more or less even spatial distribution. The constituent particles increase slightly in size for C1-2 as compared to C1-0. When homogenized at higher temperature (C1-3), constituent particles were observed to grow to 1.10μm.

Table 1 The electrical conductivity, concentrations of solutes, diameter and number density of particles [19]

	Electrical conductivity (m/Ωmm^2)	Concentration of Mn (wt%)	Constituent particles		Dispersoids	
			Diameter (μm)	Number density (mm^{-2})	Diameter (μm)	Number density (mm^{-2})
C1-0	23.9	0.35	0.88	2.8e4	-	-
C1-2	27.5	0.16	0.96	2.9e4	0.054	1.3e6
C1-3	29.0	0.11	1.10	2.1e4	0.127	5.5e4

3.2 The effect of microchemistry state on the evolution of microstructure and texture

The annealing behavior of the samples cold-rolled to $\varepsilon = 1.6$ in terms of hardness and electrical conductivity evolution during annealing at 400ºC is shown in Fig.1. Recrystallization kinetics becomes faster when the content of Mn in solid solution prior to annealing decreases from C1-0 to C1-3 (Fig.1a). This is accompanied by a decreasing amount of concurrent precipitation from C1-0 to C1-3, as indicated by the variation in electrical conductivity in Fig.1b.

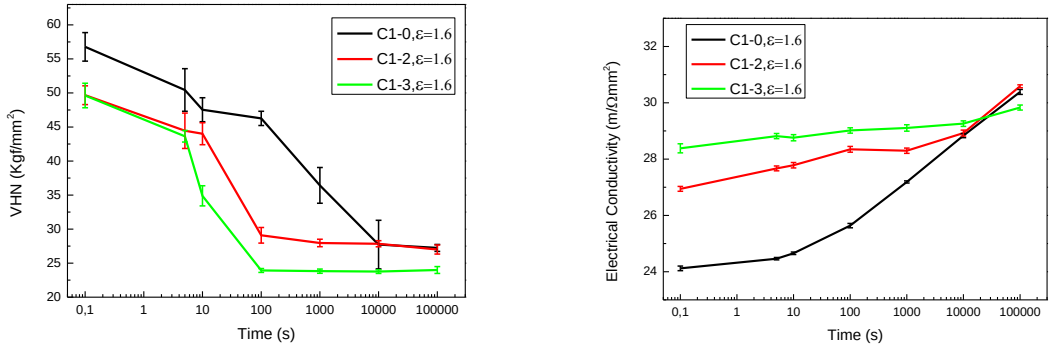

Fig.1 Variation of hardness and electrical conductivity during annealing at 400ºC for the three variants cold-rolled to $\varepsilon = 1.6$
a) Hardness; b) Electrical conductivity

The microstructure and texture evolution during annealing of the cold-rolled ($\varepsilon = 1.6$) C1-0 samples are shown in Figs. 2 and 3, respectively. As shown in Fig. 2a, even though there are no pre-existing dispersoids, any indications of recrystallization was not observed in the first 10s of annealing at 400ºC, suggesting a long incubation time and/or a time dependent nucleation behavior rather than site saturated nucleation. A typical rolling texture was obtained at this annealing stage, as illustrated in Fig. 3a. After a longer annealing time of 100s, a limited number of recrystallized grains have emerged (see Fig.2b), being parts of a few elongated "icelands" of recrystallized material. As observed these grains are already quite large before any visible nuclei have been created at other part of the sample, indicating a heterogeneous nucleation behavior. The strength of the deformation texture components have decreased, however, no clear recrystallization texture components have shown up, most probably since the volume fraction of recrystallized grains is still small (Fig.3b). These recrystallized grains then continue to grow with further annealing together with nucleation and growth of recrystallized grains at other places (Fig.2c) in the material. Growth preferentially takes place in the RD direction, indicating that concurrent precipitation, mainly on old (high angle) grain boundaries [30], aligned along the rolling direction, is exerting a dragging force along the ND direction, resulting in the elongated grain shape. A ND rotated cube texture component has shown up, together with indications of P texture (split in two peaks), both components typically observed when concurrent precipitation interacts with recrystallization [29,30]. It should be noted that, after 1000s annealing, recrystallization is not completed yet and a significant Brass texture component is still present.

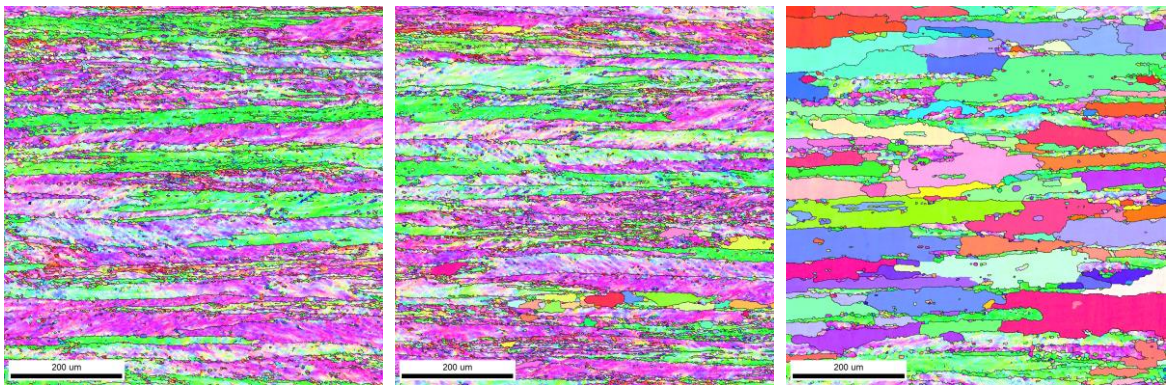

Fig.2 EBSD maps showing the microstructure of the three variants during annealing at 400°C
a) C1-0, ε =1.6, t=10s; b) C1-0, ε =1.6, t=100s; c) C1-0, ε =1.6, t=1000s.

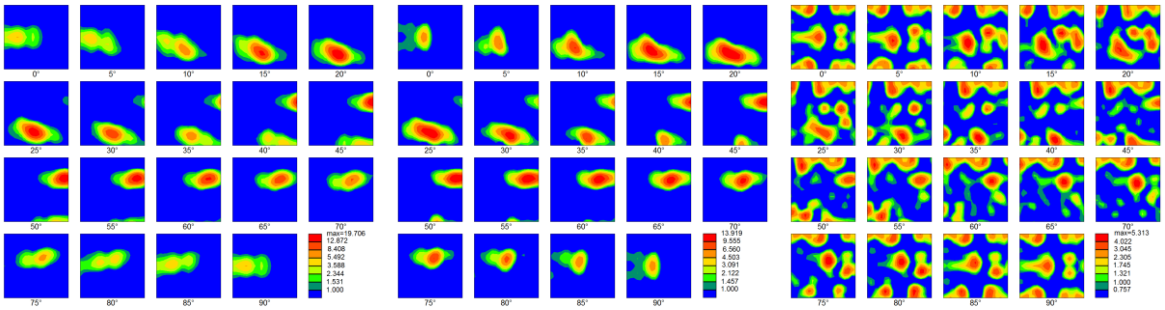

Fig.3 ODF maps showing the texture of the three variants during annealing at 400°C
a) C1-0, $\mathcal{E}$ =1.6, t=10s; b) C1-0, $\mathcal{E}$ =1.6, t=100s; c) C1-0, $\mathcal{E}$ =1.6, t=1000s.

For the deformed samples of variant C1-2, which has a large number of fine pre-existing dispersoids but lower Mn concentration in solid solution, faster recrystallization was observed when annealing at the same temperature of 400ºC, as can be seen in Fig. 4. Different from variant C1-0 (see Fig.2a), a considerable amount of recrystallized grains are already present after annealing for 10s, and as observed these grains are slightly elongated along the RD direction (Fig.4a). This difference must be due to the distinctly different microchemistry states since the thermo-mechanical processing conditions are the same. The faster recrystallization kinetics for the C1-2 sample within the first 10s indicates that pre-existing dispersoids have a less profound retarding effect on recrystallization than concurrent precipitation of Mn-containing dispersoids of a similar amount Mn. Although the dispersoids resulting from concurrent precipitation are formed at a later stage than the pre-existing ones, and during annealing, their effect on recrystallization is clearly stronger. This observation can be due to several aspects. Firstly it may be speculated that early precipitation in C1-0 (before onset of recrystallization) give rise to a high density of very small dispersoids which may provide a higher Zener drag (at this stage) in this alloy than the pre-existing ones in C1-2, more strongly suppressing nucleation than in the latter. Although a similar amount of early precipitation/removal of Mn from solid solution also take place in C1-2 (cf. Fig. 1b), it may be assumed, in this case, that Mn is mainly consumed by the already existing dispersoids causing mainly coarsening and not new small ones, thus explaining the different effect on the nucleation of recrystallization. Secondly, the fact that these two ~~types~~ populations of dispersoids are differently distributed in the material most probably also play a role. The pre-existing dispersoids are more randomly distributed [19], while concurrent precipitation mainly occurs at deformed old grain boundaries (along the RD direction) around which nucleation is very active, leading to less nucleation and a directional dragging force.

The texture in this condition (10 s annealing) is still mainly dominated by deformation texture components, although a weak ND-rotated cube component is also visible, as indicated in Fig.5a. Recrystallization completed after annealing for 100s for C1-2 (see Fig.4b). Since mainly more grains and not distinctly larger grains are observed after 100s of annealing as compared to 10s (Fig. 4b vs 4a), additional nucleation must have taken place, i.e. again in support of the assumption of some kind of time dependent nucleation, resulting in an average recrystallized size of ~43µm, much less than that of the recrystallized state of the C1-0 sample. Regarding the texture, the deformation texture is now replaced by a distinct cube texture component (with some TD-rotation), as shown in Fig.5b. Further annealing at this temperature does not change the grain shape and size (~43µm), as can be seen in Fig.4c. The evolution of texture is not significant, except that the TD rotation mainly disappear and indications of very weak P component appear (Fig.5c).

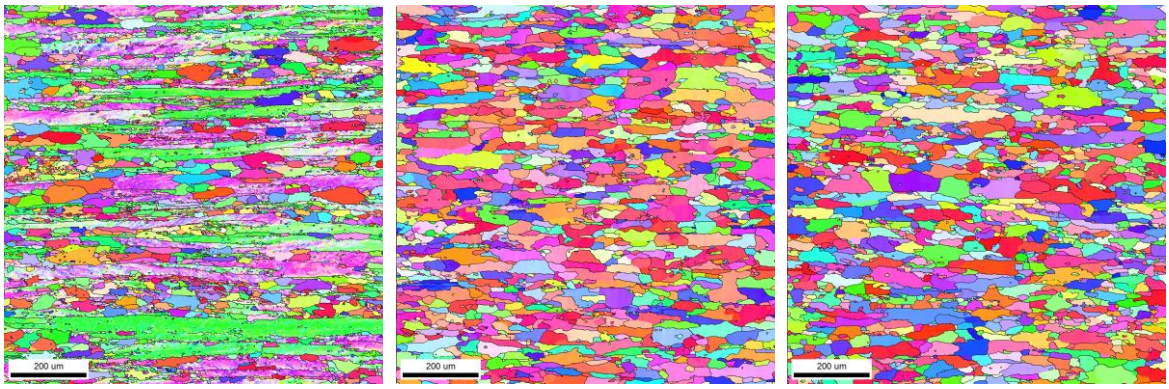

Fig.4 EBSD maps showing the microstructure of the three variants during annealing at 400°C
a) C1-2, $\mathcal{E}$ =1.6, t=10s; b) C1-2, $\mathcal{E}$ =1.6, t=100s; c) C1-2, $\mathcal{E}$ =1.6, t=1000s.

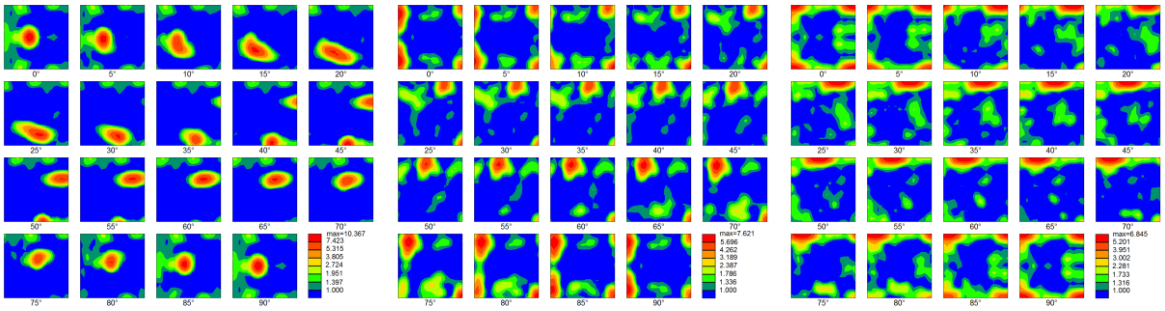

Fig.5 ODF maps showing the texture of the three variants during annealing at 400°C
a) C1-2, $\mathcal{E}$ =1.6, t=10s; b) C1-2, $\mathcal{E}$ =1.6, t=100s; c) C1-2, $\mathcal{E}$ =1.6, t=1000s.

The fastest recrystallization kinetics was observed for the C1-3 samples, as previously shown in Fig.1a, this can be ascribed to their limited number of pre-existed dispersoids and the lowest Mn content prior to annealing, both factors which imply a negligible contribution to any precipitation-recrystallization interactions. A large number of recrystallized grains were present already after annealing for 10s, with mainly equiaxed shape, as seen in Fig.6a. Still the deformation texture outweighs indications of any recrystallization texture components, such as the very weak Cube and Goss components also present in Fig.7a. Annealing to longer times at 400^{o}C leads to fully recrystallized structures, with an average grain size of ~21 μm, as shown in Figs. 6b and c. The texture of the recrystallized samples is dominated now by the cube component, while typical deformation texture components still exist, even though they diminish with longer annealing times, as seen in Figs.7b and c. The texture intensity is in general weaker than that of the C1-2 samples annealed at the same conditions, as well as the recrystallization texture of the same variants after larger deformation [19].

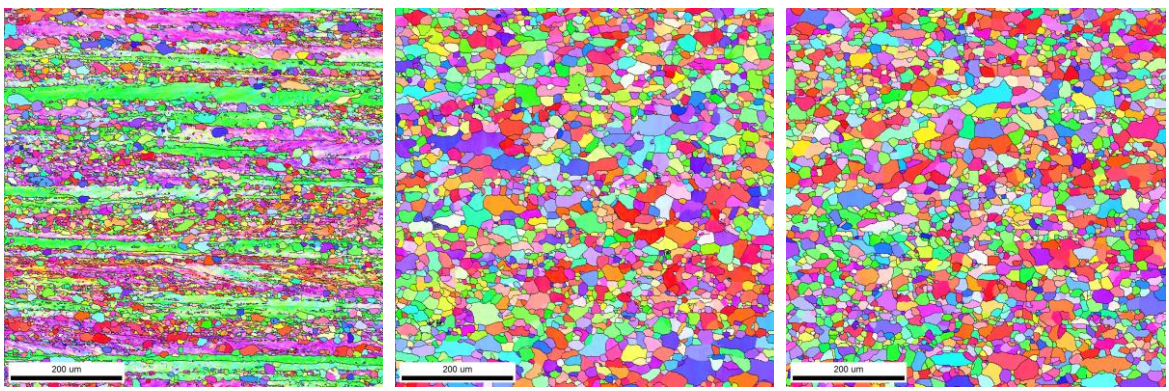

Fig.6 EBSD maps showing the microstructure of the three variants during annealing at 400°C

a) C1-3, $\mathcal{E}$ =1.6, t=10s; b) C1-3, $\mathcal{E}$ =1.6, t=100s; c) C1-3, $\mathcal{E}$ =1.6, t=1000s.

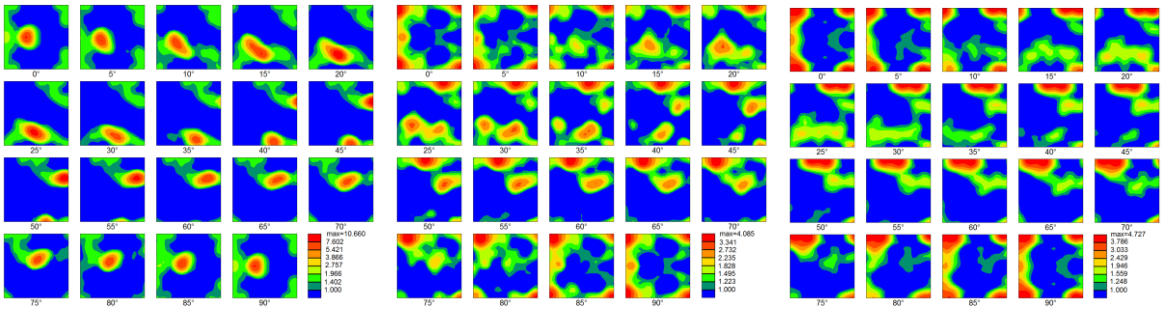

Fig.7 ODF maps showing the texture of the three variants during annealing at 400°C

a) C1-3, $\mathcal{E}$ =1.6, t=10s; b) C1-3, $\mathcal{E}$ =1.6, t=100s; c) C1-3, $\mathcal{E}$ =1.6, t=1000s.

4 Conclusions

Microstructural evolution of a cold-rolled Al-Mn-Fe-Si alloy, with various microchemistry states introduced by different homogenization procedures during annealing after cold rolling deformation has been studied. It is clearly demonstrated that the microchemistry state may strongly affect the recrystallization kinetics, as well as recrystallization grain structure and texture.

1) The microchemistry state has a profound effect on the initial stage of recrystallization. High level of Mn content in solid solution gives significant concurrent precipitation, which suppresses nucleation and only a limited number of recrystallized grains are present with elongated shape due to the exerting dragging force along the ND direction from the concurrent precipitation. Large number of equiaxed grains is nucleated when the concentration level of Mn in solid solution is low, due to less retarding force from the dispersoids.

2) The microchemistry state also affects recrystallization kinetics. Strong concurrent precipitation strongly suppresses nucleation and retard recrystallization, while the fastest recrystallization is obtained when both the concurrent precipitation and pre-existing dispersoids are less. It is indicated that pre-existing dispersoids have less effect on recrystallization than concurrent precipitation during annealing.

3) ND-rotated cube and P components are the dominant texture components when strong concurrent precipitation (relatively high concentration level of Mn prior to annealing) interacts with recrystallization. On the other side, the recrystallization texture is characterized by a distinct cube texture with same deformation texture components when the interaction between fine dispersoids (pre-existed and concurrently precipited) and recrystallization is avoided (low content of Mn in solid solution).

Acknowledgments

This research work has been supported by the KMB project (193179/I40) in Norway. The financial support by the Research Council of Norway and the industrial partners, Hydro Aluminium and Sapa Technology is gratefully acknowledged. KH acknowledges the financial support from NTNU, through the Strategic Area Materials.

References

[1] Humphreys F J. The nucleation of recrystallization at second phase particles in deformed aluminium [J]. Acta Metallurgica, 1977, 25(11):1323-1344.

[2] Doherty R D, Hughes D A, Humphreys F J, Jonas J J, Jensen D J, Kassner M E et al. Current issues in recrystallization: a review [J]. Materials Science and Engineering A, 1997, 238(2): 219-274.

[3] Humphreys F J. A unified theory of recovery, recrystallization and grain growth, based on the stability and growth of cellular microstructures-I. The basic model [J]. Acta Materialia, 1997, 45(10):4231-4240.

[4] Humphreys F J. Particle stimulated nucleation of recrystallization at silica particles in nickel [J]. Scripta Materialia, 2000, 43(7):591-596.

[5] Daaland O, Nes E. Recrystallization texture development in commercial Al-Mn-Mg alloys [J]. Acta Materialia, 1996, 44(4):1413-1435.

[6] Zhang Y H, Juul Jensen D, Zhang Y B, Lin F X, Zhang Z Q, Liu Q. Three-dimensional investigation of recrystallization nucleation in a particle-containing Al alloy [J]. Scripta Materialia, 2012, 67(4):320-323.

[7] Nes E, Ryum N, Hunderi O. On the Zener drag [J]. Acta Metallurgica, 1985, 33(4):11-22.

[8] Humphreys F J, Hatherly M, Recrystallization and Related Annealing Phenomena [M], Second ed. Oxford, United Kingdom: Elsevier science Ltd, 2004.

[9] Humphreys F J, Kalu PN. Dislocation-particle interactions during high temperature deformation of two-phase aluminium alloys [J]. Acta Metallurgica, 1987, 35(12):2815-2529.

[10] Hutchinson W B, Oscarsson A, Karlsson Å. Control of microstructure and earing behaviour in aluminium alloy AA 3004 hot bands [J]. Materials Science and Technology, 1989, 5(11):1118-1127.

[11] Osman M, Engler O, Karhausen K, Löchte L, McLaren A J. Effect of homogenisation conditions on recrystallisation in Al-Mg-Mn alloy AA 5454. Materials Science and Technology, 2007, 23(6): 688-698.

[12] Engler O, Liu Z, Kuknke K. Impact of homogenization on particles in the Al–Mg–Mn alloy AA 5454 - experiment and simulation [J]. Journal of Alloys and Compounds, 2013, 560(25):111-122

[13] Engler O, Laptyeva G, Wang N. Impact of homogenization on microchemistry and recrystallization of the Al-Fe-Mn alloy AA 8006 [J]. Materials Characterization, 2013, 79: 60-75.

[14] Birol Y. Impact of homogenization on recrystallization of a supersaturated Al-Mn alloy [J]. Scripta Materialia, 2009, 60(1):5-8.

[15] Birol Y. Optimization of homogenization for a low alloyed AlMgSi alloy [J]. Materials Characterization, 2013, 80:69-75.

[16] Totik Y, Gavgali M.The effect of homogenization treatment on the hot workability between the surface and the center of AA 2014 ingots [J]. Materials Characterization, 2002, 49:261-268.

[17] Radetic T, Popovic M, Romhanji E. Microstructure evolution of a modified AA5083 aluminum alloy during a multistage homogenization treatment [J]. Materials Characterization, 2012, 65:16-27.

[18] Du Q, Poole W J, Wells M A, Parson N C. Microstructure evolution during homogenization of Al-Mn-Fe-Si alloys: Modeling and experimental results [J]. Acta Materialia, 2013, 61(13):4961-4973.

[19] Huang K, Wang N, Li YJ, Marthinsen K. The effect of homogenization and amount of Mn on the softening behavior of cold-rolled Al-Mn-Fe-Si alloys. (Submitted to Mater Charact)

[20] Huang K, Li Y J, Marthinsen K. Isothermal and non-isothermal annealing of cold-rolled Al-Mn-Fe-Si alloy with different microchemistry states. (Submitted to Thermec' 2013)

[21] Huang K, Li Y J, Marthinsen K. Non-isothermal annealing of a cold-rolled Al-Mn-Fe-Si alloy with different microchemistry states. (In preparation)

[22] Huang K, Li Y J, Marthinsen K. Investigation of recrystallization in a cold-rolled Al-Mn-Fe-Si alloy through isothermal and non-isothermal heating experiments – A comparative study. (In preparation)

[23] Wang N, Flatøy J E, Li Y J, Marthinsen K. Evolution in microstructure and mechanical properties during back-annealing of AlMnFeSi alloy [J]. Transactions of Nonferrous Metals Society of China, 2012, 22:1878-1883.
[24] Wang N, Li Y J, Marthinsen K. Characterization the softening behavior of cold rolled AlMnFeSi-alloys during conditions of concurrent precipitation [J]. Materials Science Forum. 2013,753:231-234.
[25] Wang N, Li Y J, Marthinsen K. Softening behavior of cold rolled Al-Mn-Fe-Si-alloys during conditions of concurrent precipitation. To be submitted
[26] Wang N, Li Y J, Marthinsen K. The influence of dispersoids and concurrent precipitation on the Softening behavior of cold rolled Al-Mn-Fe-Si-alloys. To be submitted.
[27] Muggerud A M F, Mørtsell E A, Li Y J, Holmestad R. Dispersoid strengthening in AA3xxx alloys with varying Mn and Si content during annealing at low temperatures [J]. Materials Science and Engineering A 2013, 567(1):21-28
[28] Li Y J, Arnberg L, Evolution of eutectic intermetallic particles in DC-cast AA3003 alloy during heating and homogenization [J]. Materials Science and Engineering A 2003, 347(1-2): 130-135
[29] Tangen S, Sjølstad K, Furu T, Nes E. Effect of concurrent precipitation on recrystallization and evolution of the P-texture component in a commercial Al-Mn alloy [J]. Metallurgical and Materials Transactions A 2010, 41(11):2970-2983
[30] Somerday M, Humphreys F J., Recrystallization behavior of supersaturated Al-Mn alloys Part 1-Al-1.3wt-% Mn [J]. Materials Science and Technology, 2003,19: 20-29

关于冷轧不同微量化学状态 Al–Mn-Fe-Si 铝合金的等温退火研究

黄科[1]，李彦军[1,2]，Knut Marthinsen[1]

1. Department of Materials Science and Engineering, Norwegian University of Science and Technology (NTNU), Trondheim 7491, Norway；
2. SINTEF Materials and Chemistry, N-7465, Norway

本文通过三种不同热处理工艺使一种 Al-Mn-Fe-Si 合金获得了不同尺寸和数量的固溶度和弥散析出相，包括铸造状态，一种富含高密度、细小弥散相的状态，另外一种状态则仅有少量、相对粗大的弥散相。采用 EBSD 技术系统研究了冷轧后退火过程中微观组织的演变以及初始组织状态对再结晶动力学，再结晶晶粒形貌和织构的影响。研究表明再结晶动力学，最终微观组织和织构由加工条件和合金的初始组织和固溶度决定。强烈的弥散析出相阻止形核，显著阻碍软化过程，最终得到粗大的狭长晶粒以及 P 和 ND-rotated cube 织构。在没有预先存在的细小、稠密的弥散相并且在退火搓成中弥散相析出数量很少的时候则能更快完成再结晶并得到均匀、细小的等轴晶以及显著 Cube 织构。

关键词：Al–Mn-Fe-Si 铝合金；再结晶；微量化学；颗粒；析出相；再结晶织构